JOURNAL OF MATERIALS SCIENCE 35 (2000) 4501–4505

# $\gamma \leftrightarrow \alpha_2$ Phase transformation in fractured high temperature stress rupture Ti-48Al-2Nb(at.%)

Z. Y. CHENG, X. W. DU, JING ZHU*
*Electron Microscopy Laboratory, School of Materials Science and Engineering, Tsinghua University, Beijing 100084, People's Republic of China*
*E-mail: jzhu@mail.tsinghua.edu.cn*

C. X. CAO, F. S. SUN
*Aeronautical Materials Research Institute of Beijing, Beijing 100095, People's Republic of China*

The $\gamma \leftrightarrow \alpha_2$ phase transformation in fractured high temperature stress rupture Ti-48Al-2Nb(at.%) alloy has been studied by analytical electron microscopy. $\alpha_2$ and $\gamma$ phases were found at grain boundaries. $\alpha_2$ layers that suspended in $\gamma$ layers and interfacial ledge higher than $2d_{(111)\gamma}$ at $\gamma/\alpha_2$ interfaces were observed in the lamellar grains. These facts indicated that $\gamma \leftrightarrow \alpha_2$ phase transformation and dynamic recrystallization have occurred during high temperature stress rupture deformation. It can be concluded that deformation induced $\gamma \leftrightarrow \alpha_2$ phase transformation and dynamic recrystallization resulted in the presence of $\gamma$ particles at grain boundaries. A structural and compositional transition area between deformation-induced $\alpha_2$(or $\gamma$) and its adjacently original $\gamma$(or $\alpha_2$) phases was found by HREM and EDS and is suggested as a way to transform between $\gamma$ and $\alpha_2$ phase during high temperature stress rupture deformation. The transition area was formed by slide of partial dislocations on close-packed planes and diffusion of atoms.


## 1. Introduction

The Ti-Al intermetallics are potentially good high-temperature structural materials, mainly due to their high modulus retention , low density and oxidation resistance at elevated temperatures [1]. The deformation behavior and mechanisms at ambient temperature have been extensively studied. Accompanying deformation there are some deformation-induced phase transformations, including $\gamma \rightarrow \alpha_2$ and $\alpha_2 \rightarrow \gamma$ [2–4]. $\gamma \rightarrow \alpha_2$ phase transformations have also been observed in hot-forged Ti-Al-Nb(at.%) [5]. Recently, intensive investigations of creep behavior and mechanisms in Ti-Al intermetallics have being conducted [6–12]. The creep behavior of materials depends strongly on their microstructures, which can be optimized and designed through the proper control of processing and alloying. Thus some studies focussed on the effect of microstructure on creep properties and changes in microstructure during creep [10, 11, 13, 14–16].

The present paper reports the investigation of microstructural changes and $\gamma \leftrightarrow \alpha_2$ phase transformation observed in fractured high-temperature stress rupture Ti-48Al-2Nb(at.%) duplex alloy by conventional and high resolution techniques of transmission electron microscopy.

## 2. Experimental procedure

A conventional tungsten-arc-melting technique was employed to prepare the Ti-48Al-2Nb(at.%) alloy. Subsequently, the material was heat treated according the following schedules: (1) annealing at 1200°C for 12 h and then air cooling (2) annealing at 900°C for 8 h and then air cooling. The material was deformed at a temperature of 800°C under a stress of 250 MPa to failure at 130 h. To investigate the microstructural changes of the alloy during high temperature stress rupture deformation, samples have been prepared as follows: slices about 0.3 mm in thickness were cut, perpendicular to the deformation axis, from the position adjacent to the failure section (here referred to as deformed sample) and the fixed end of the fractured specimen (here referred to as undeformed sample), respectively, as shown in Fig. 1. The slices were mechanically ground and then thinned by twin-jet polishing. The polished specimens were then examined using a JEM-2010F field emission analytical transmission electron microscope attached with an EDS (Energy Dispersive Spectrometer Link ISIS) system.

## 3. Experimental results and discussion

### 3.1. $\gamma \rightarrow \alpha_2$ phase transformation and dynamic recrystallization at grain boundaries

Conventional TEM observations indicate that the TiAl sample used in the present study shows a duplex microstructure. The undeformed sample in the present study was taken from the fixed end of the fractured high temperature stress rupture specimen, so the undeformed

* Author to whom all correspondence should be addressed.

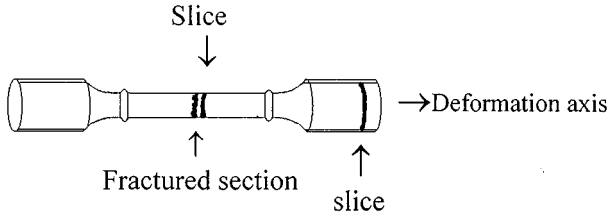


*Figure 1* A schematic illustration of the specimens studied.

sample may be considered as a aged sample (at 800°C for 130 h). In the undeformed sample, no $\alpha_2$ and $\gamma$ particles precipitate at grain boundaries, as shown in Fig. 2a. This implies that $\gamma \leftrightarrow \alpha_2$ phase transformation at grain boundaries didn't occur with aging. Significant microstructural difference of grain boundaries has been detected in the deformed sample compared with the undoformed sample (see Fig. 2b). The experimental results from the combination of SAD (selected area diffraction) patterns and EDS confirmed that the deformed sample contains $\alpha_2$ and $\gamma$ particles at the boundaries $\gamma_e/\gamma_e$, $\gamma_e$/L and $\gamma$ particles appeared at the grain boundaries L/L ($\gamma_e$: equiaxed $\gamma$ grain, L: lamellar grain). A summary of $\alpha_2$ and $\gamma$ phases precipitates at grain boundaries is given in Table I.

Considering the low stacking energy of binary TiAl alloy [17, 18] and findings on dynamic recrystallization in some TiAl alloy during creep [10, 15], the new $\gamma$ particles at grain boundaries $\gamma_e/\gamma_e$, $\gamma_e$/L and L/L might be attributed to dynamic recrystallization during high temperature stress rupture deformation. According to these facts that no occurrence of $\gamma \rightarrow \alpha_2$ phase transformation with aging and the appearance of $\alpha_2$ phase at grain boundaries in the deformed alloy, it can be confirm that deformation induced $\gamma \rightarrow \alpha_2$ phase transformation at grain boundaries in Ti-48Al-2Nb(at.%) alloy during high temperature stress rupture deformation.

To understand how deformation-induced $\gamma \rightarrow \alpha_2$ phase transformation takes place, HREM observation and microanalysis of composition are performed. One of the examples shows in Figs. 3–5. The upper left corner of Fig. 3a shows a morphology of a deformation-induced $\alpha_2$ precipitate at the $\gamma_e$/L boundary. $E_s$ denotes one side of the $\alpha_2$ precipitate, close to the equiaxed $\gamma_e$ grain. The other side of the $\alpha_2$ precipitate adjacent to the $\gamma$ layer in a lamella, is marked as $L_s$. HREM images of the sides $L_s$ and $E_s$ of the $\alpha_2$ phase, viewed along the $[1120]_{\alpha 2}$ direction, are shown in Fig. 3 and Fig. 5, respectively. The HREM image of the side $L_s$ (see Fig. 3a) shows that there existed a transition layer (marked as T) between the perfect $\alpha_2$ precipitate and $\gamma$ layer in the lamella. The structure of the transition layer T is different from perfect $\alpha_2$ or $\gamma$ phases. The HREM image (Fig. 5) of the side $E_s$, on the other hand, shows no transition layer such as layer T between the $\alpha_2$ precipitate and $\gamma$ equiaxed grain. The thickness of layer T in Fig. 3a is about 5 nm. Figs. 3b and 3c are enlargements of layer T. Layer T consists of two types of areas (marked P and F, respectively) revealing different

TABLE I Summary of deformation-induced $\alpha_2$ and $\gamma$ phase at grain boundaries

| type of a grain boundary and deformation-induced phases at grain boundaries | composition of deformation-induced phases at grain boundaries(at.%) | | | | | |
|---|---|---|---|---|---|---|
| | $\alpha_2$ | | | $\gamma$ | | |
| | Ti | Al | Nb | Ti | Al | Nb |
| 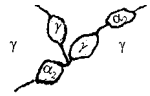 | 65.68 | 32.47 | 1.85 | 49.40 | 48.09 | 2.51 |
| 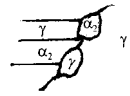 | 60.79 | 37.34 | 1.87 | 48.74 | 49.18 | 2.08 |
| 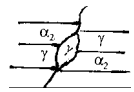 | - | - | - | 49.06 | 48.44 | 2.50 |

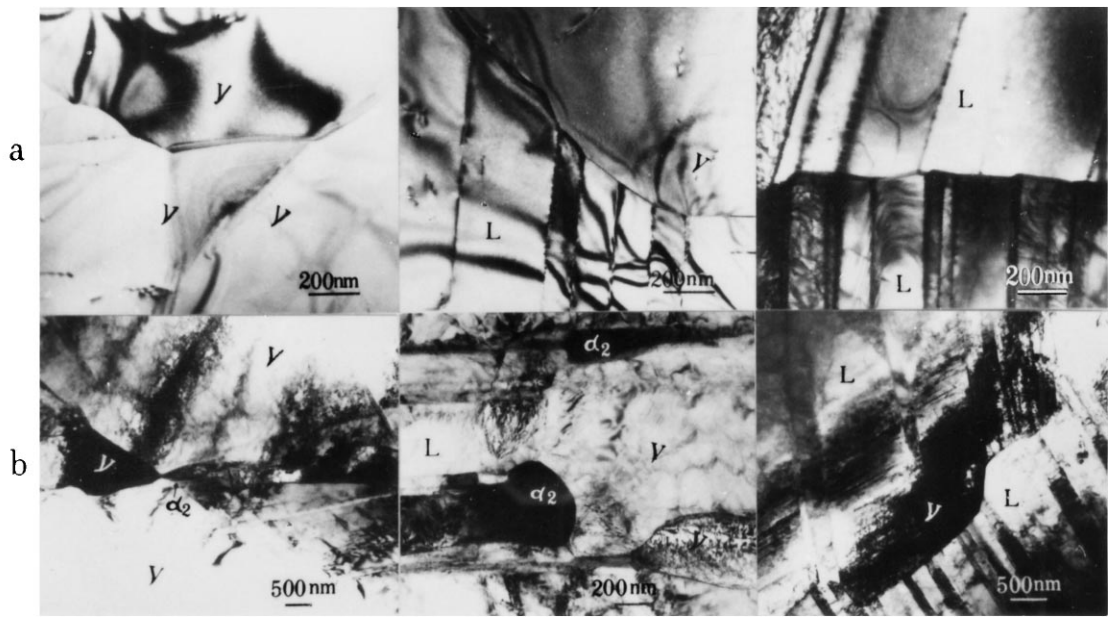


*Figure 2* Morphology of grain boundaries in Ti-48Al-2Nb(at.%) alloys. (a) undeformed, (b) high temperature stress rupture fractured. $\alpha_2$ and $\gamma$ phases were found at grain boundaries in the deformed alloy.

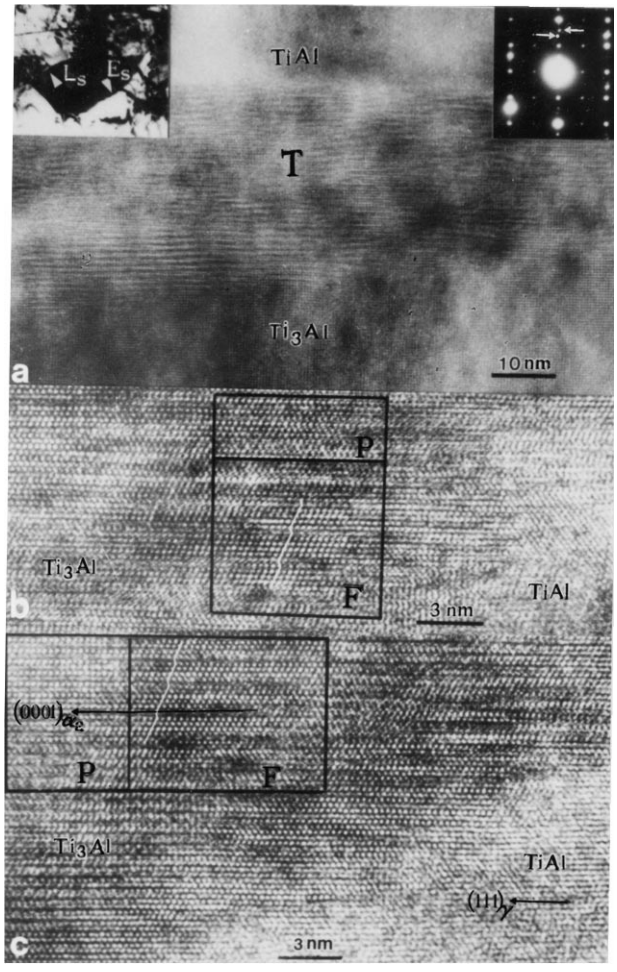


*Figure 3* HREM images of the $L_s$ side of the $\alpha_2$ phase (a) showing the transition layer T between perfect $\alpha_2$ and $\gamma$ phases, viewed along the $[1120]_{\alpha 2}$ direction. An image of the $\alpha_2$ phase at a grain boundary $\gamma_e$/L is shown in the upper left corner. (b) and (c) enlargements of the transition layer T in Fig. 2a presenting a stacking-fault-like structure.

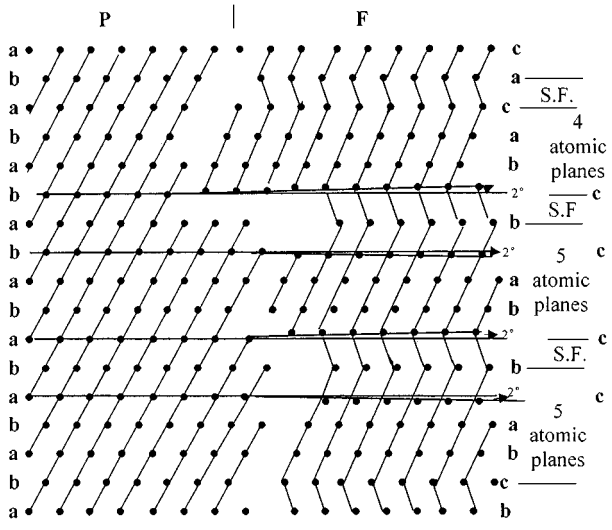


*Figure 4* A schematic diagram showing the stacking-fault-like structure in the transition layer T in Fig. 3.

HREM images under the same defocus conditions and thickness. The HREM images of the P areas in Figs. 3b and 3c show the structure of a perfect $\alpha_2$ phase. Further examination of the HREM images of areas F in Figs. 3b and 3c reveals an abc stacking sequence of $\gamma$ phase with stacking faults every 4, 5 or 6 atomic planes, as

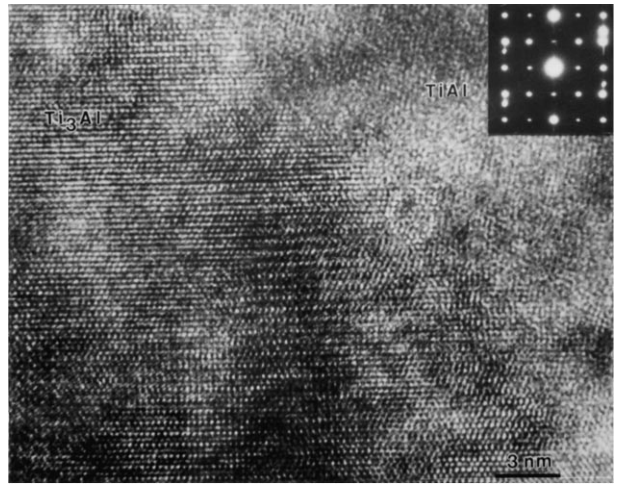


*Figure 5* HREM image of the side $E_s$ of the $\alpha_2$ precipitate (shown at upper left in Fig. 3a). No transition layer is found between perfect $\alpha_2$ precipitate and the equiaxed $\gamma_e$ grain.

shown schematically in Fig. 4 (a, b and c are close-packed planes). Therefore the layer T may be considered as the result of the slide of partial dislocations on close-packed planes. Consequently, abab stacking sequences of $\alpha_2$ phase was obtained near those stacking fault planes. Slide of partial dislocations went on in the regions with abc stacking sequences in the layer T during deformation, the stacking structure of $\alpha_2$ phase might be ultimately formed. It can be also seen from Figs 3b and 3c that the atomic planes next to the stacking fault planes exhibit a misorientation angle of about $2^\circ$ with the $(0001)_{\alpha 2}$ plane. These atomic planes contribute the diffraction spots indicated by white arrows in the diffraction pattern at the upper right corner of Fig. 3a.

EDS spectra were acquired from side $E_s$, the areas F of side $L_s$, and $\gamma$ grain adjacent to sides $E_s$ and $L_s$. An electron beam with a 1.6 nm diameter was used. The results of microanalysis of these areas were listed in Table II. It is clearly seen from the Table II that the composition of area F is different from that of the $\alpha_2$ precipitate and $\gamma_e$ grain. The result of microanalysis demonstrates that atoms were diffusing to generate the correct composition and ordering of $\alpha_2$ phase along with slide of partial dislocations on close–packed planes.

### 3.2. $\gamma \leftrightarrow \alpha_2$ phase transformation in lamellar grains

As can be seen in Fig. 6, the microstructure of lamellar grains in the deformed sample is significantly

TABLE II The composition of the sides $E_s$ and $L_s$ of the $\alpha_2$ particle, $\alpha_2$ and $\gamma$ phase

| | Ti (at.%) | Al (at.%) | Nb (at.%) |
|---|---|---|---|
| Area F on the | | | |
| side $L_s$ | 54.97 | 42.30 | 2.73 |
| side $E_s$ | 63.52 | 33.79 | 2.69 |
| $\gamma_e$ grain | 48.07 | 48.97 | 2.96 |
| $\alpha_2$ precipitate | 63.35 | 33.78 | 2.87 |

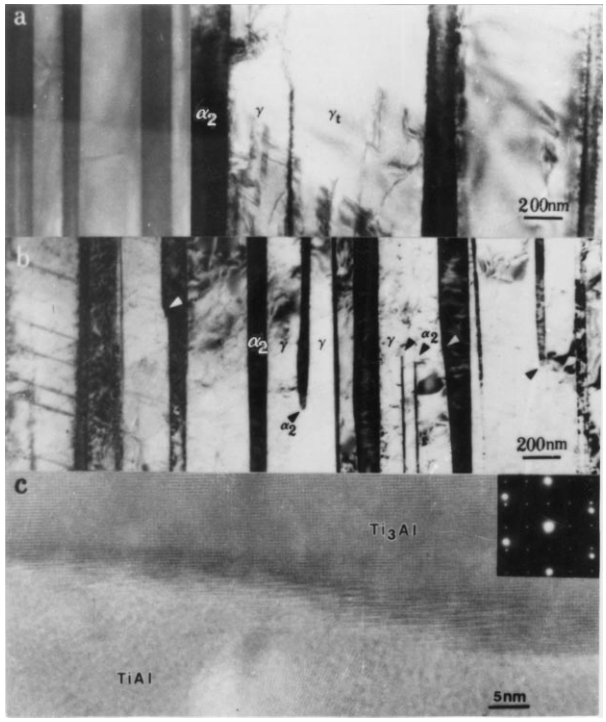


*Figure 6* Lamellar structure with $\alpha_2$ and $\gamma$ layers in Ti-48Al-2Nb(at.%) alloys. (a) undeformed, (b) high temperature stress rupture fractured. (c) An enlargement of $\alpha_2$ ledges indicated by white arrows in Fig. 6b.

different from that observed in the undeformed sample. Similar to results reported previously in Ti-Al intermetallics [19], many $\alpha_2$ layers (designated with black arrows in Fig. 6) suspended in wider $\gamma$ layers and higher ledges at $\alpha_2/\gamma$ interfaces (indicated by white arrows in Fig. 6) were observed. These changes of morphology in lamellar grains illustrate that $\gamma \leftrightarrow \alpha_2$ phase transformation also occurred in lamellar grains during high temperature stress rupture deformation. Based on the same analysis as $\gamma \rightarrow \alpha_2$ phase transformation at grain boundaries, it can thought that deformation resulted in $\gamma \leftrightarrow \alpha_2$ phase transformation in lamellar grains.

TABLE III The composition of the tip of a $\alpha_2$ layer and the adjacent $\alpha_2$ and $\gamma$ layers

| | Ti (at.%) | Al (at.%) | Nb (at.%) |
|---|---|---|---|
| The tip of a $\alpha_2$ layer | 52.01 | 45.50 | 2.49 |
| Adjacent $\gamma$ layer | 48.91 | 48.67 | 2.42 |
| Adjacent $\alpha_2$ layer | 63.08 | 34.68 | 2.24 |

Fig. 7 shows the HREM image of the tip of a $\alpha_2$ layer suspended in a $\gamma$ lamella. It can be seen clearly in Fig. 7 that the HREM image of the small transition area (marked as S) at the tip of the $\alpha_2$ lamella is very much different from the adjacent $\gamma$ and $\alpha_2$. The stacking sequence of the area S is . . . ab′cbc′b. . ., which is similar to or identical to that of $Ti_2Al$ phase in Al-rich TiAl alloy reported previously [20–22]. The length of the area S along the $\alpha_2$ layer is about 12 nm. It is also noted that due to the area S is really small thus the SAD pattern (shown at the upper right corner in Fig. 7), taken from the region including the area S, $\alpha_2$ and $\gamma$ phase, shows no other spots except those for $\alpha_2$ and $\gamma$ phases. This may be the reason why the transition area S has not been reported up to now. Table III presents the composition of area S, and the $\alpha_2$ and $\gamma$ phases close to area S. The diameter of the electron beam used was 1.6 nm. The composition of area S corresponds to area F in Fig. 3c. The ratio of Ti to Al in the area S is higher than that of $\gamma$ phase and lower than that of $\alpha_2$ phase. Similar to the discussion of $\gamma \rightarrow \alpha_2$ phase transformation at grain boundaries, it is suggested that $\gamma \leftrightarrow \alpha_2$ phase transformation in lamellar grains was finally accomplished by forming the transition area S and atomic diffusion. The transition area S was formed by slide of partial dislocations on close-packed planes and atomic diffusion.

## 4. Conclusions

(1) Deformation induced $\gamma \rightarrow \alpha_2$ phase transformation at grain boundaries and $\gamma \leftrightarrow \alpha_2$ phase transformation

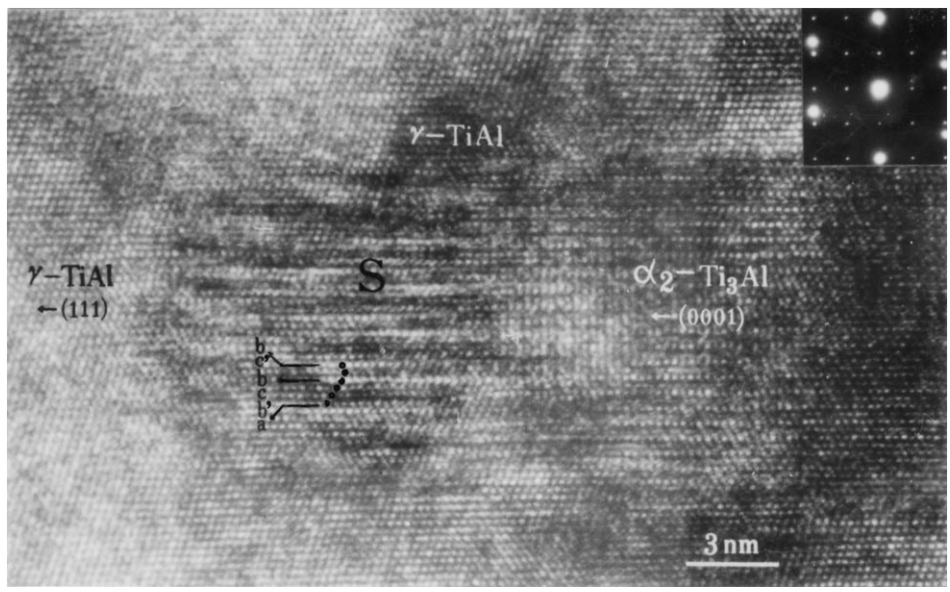


*Figure 7* HREM image of the tip of an $\alpha_2$ layer suspended in a $\gamma$ layer: the image was viewed along the $[110]_\gamma//[1120]_{\alpha 2}$ direction. The HREM image shows a transition area (marked S) with the stacking sequence . . . ab′cbc′b. . . that is the same as that attributed to the $Ti_2Al$ phase.

in lamellar grains during high temperature stress rupture deformation. $\gamma \leftrightarrow \alpha_2$ phase transformation at grain boundaries didn't be found with aging.

(2) Dynamic recyrstallization took place and resulted in the presence of small $\gamma$ phases at grain boundaries during high temperature stress rupture deformation.

(3) There exists a transition area between deformation-induced $\gamma$ or $\alpha_2$ precipitates and original $\alpha_2$ or $\gamma$ phases. The stacking sequence and composition of the transition area is different from that of $\gamma$ and $\alpha_2$ phases. The ratio of Ti to Al is higher than that of $\gamma$ phase and lower than that of $\alpha_2$ phase. The transition area was formed by slide of partial dislocations on close-packed planes and atomic diffusion.

(4) $\gamma \leftrightarrow \alpha_2$ phase transformation was finally accomplished by forming the transition area and atomic diffusion during high temperature stress rupture deformation.

## Acknowledgements

This work was supported by Chinese National Nature Science Foundation.

## References

1. Y. W. KIM and D. M. DIMIDUK, *JOM* **8** (1991) 40.
2. F. APPEL, P. A. BEAVEN and R. WAGNER, *Acta Metall. Mater.* **41** (1993) 1721.
3. Y. GAO, J. ZHU, H. SHEN, Y. WANG, *Scr. Metall. Mater.* **28** (1993) 651.
4. Y. G. GANG, F. D. TICHELAAR, F. W. SCHAPINK, Q. XU and C. Q. CHEN, *ibid.* **32** (1995) 981.
5. J. G. WANG, L. C. ZHANG, G. L. CHEN, H. Q. YE and T. G. NIEH, *Mater. Sci. Eng.* **A239/240** (1997) 287.
6. MIN LU and K. J. HEMKER, *Acta Mater.* **45** (1997) 3573.
7. D. I. KIMM and J. WOLFENNSTINE, *Scr. Metall. Mater.* **30** (1994) 615.
8. L. M. HSIUNG and T. G. NIEH, *Mater. Sci. Eng.* **A339-240** (1997) 438.
9. R. V. VAIDYA, ZHE JIN, C. CADY, G. T. GRAY II and D. P. BUTT, *Scr. Mater.* **41** (1999) 569.
10. M. ES-SOUNI, A. BARTELS and R. WAGNER, *Acta Metall. Mater.* **43** (1995) 153.
11. *Idem., Mater. Sci. Eng.* **A192/193** (1995) 698.
12. R. W. HAYES and P. A. MCQUAY, *Scr. Metall. Mater.* **30** (1994) 259.
13. T. T. CHENG and M. R. WILLIS, *Scr. Mater.* **39** (1998) 1255.
14. D. Y. SEO, T. R. BIELER, S. U. AN and D. E. LARSEN, *Metall. Mater. Trans. A* **29A** (1998) 89.
15. B. SKROTZKI, T. RUDOLF, A. DLOUHY and G. EGGELER, *Scri. Mater.* **39** (1998) 1545.
16. C. DERDER, R. BONNET, J. M. PÉNISSON and G. FROMMEYER, *ibid.* **38** (1997) 757.
17. G. HUG, A. LOISEAU and P. VEYSSIÉRE, *Phil. Mag.* **57** (1988) 499.
18. C. L. FU and M. H. YOO, *Scri. Mater.* **37** (1997) 1453.
19. J. N. WANG and T. G. NIEH, *Acta Metall.* **46** (1998) 1887.
20. A. LOISEAU and A. LASALONI, *Acta Cryst.* **B39** (1983) 580.
21. *Idem., Mater. Sci. Eng.* **67** (1984) 169.
22. L. L. HE, H. Q. YE, R. G. XU and D. Z. YANG, *Mater. Lett.* **19** (1994) 17.

*Received 10 November 1999*
*and accepted 2 March 2000*